Received: 21 April 2023 | Revised: 16 November 2023 | Accepted: 30 November 2023

DOI: 10.1111/jfpe.14520

ORIGINAL ARTICLE

Journal of Food Process Engineering WILEY

Systematic investigation of the influence of suspended particles on UV-C inactivation of *Saccharomyces cerevisiae* in liquid food systems

Benedikt Woll[1] | **Svetlana Cvetkova**[2] | **Volker Gräf**[1] | **Maren Scharfenberger-Schmeer**[2] | **Dominik Durner**[2] | **Mario Stahl**[1]

[1]Department of Food Technology and Bioprocess Engineering, Max Rubner-Institut, Federal Research Institute of Nutrition and Food, Karlsruhe, Germany

[2]Institute for Viticulture and Enology, Dienstleistungszentrum Laendlicher Raum (DLR) Rheinpfalz, Neustadt an der Weinstrasse, Germany

Correspondence
Benedikt Woll, Department of Food Technology and Bioprocess Engineering, Max Rubner-Institut, Federal Research Institute of Nutrition and Food, Haid-und-Neu-Straße 9, Karlsruhe 76131, Germany.
Email: benedikt.hirt@mri.bund.de

Funding information
Research Association of the German Food Industry (FEI), Grant/Award Number: AiF 20921 N

Abstract

UV-C treatment of food products is a non-thermal, energy- and cost-efficient alternative to traditional thermal treatment. To ensure a shelf-stable product, it is necessary to understand the UV-C dose–response relationship of spoilage microorganisms in liquid food. Two product parameters in particular have a significant affect on the UV-C propagation through liquid food: the absorption of dissolved substances and the absorption and scattering of suspended particles in the liquid. The aim of this study was to investigate the effect of suspended solids on the UV-C inactivation of *Saccharomyces cerevisiae* in model suspensions with different opacifiers (silicon dioxide, titanium dioxide, microcrystalline cellulose, calcium carbonate, and polymethyl methacrylate [PMMA]). PMMA spheres with 11 different diameters ranging from 100 to 6 µm were used to determine the influence of particle size on the inactivation process. Particles with a high imaginary part with respect to the refractive index at 254 nm absorb the UV-C light instead of scattering it. This energy loss results in less inactivation of *S. cerevisiae*. Non-absorbing particles affect inactivation if their size results in Mie scattering. Suspensions of particles between 500 nm and 2 µm significantly reduce the efficiency of the process. The greatest influence is seen at a size of about 900 nm, where the Mie scattering efficiency of PMMA in water is at its maximum. Suspensions with turbidity of 1000 NTU, consisting of particles larger than 2 µm, had no effect on the inactivation of *S. cerevisiae*. Particle sizes that are in the Rayleigh scattering range (<500 nm) show little to no effect on inactivation. This correlation was confirmed by inactivation experiments of *S. cerevisiae* in cloudy and clarified apple and grape juice. The results show, that the determination of the particle size distribution and its ratio to the wavelength is crucial for predicting the efficiency of microorganism inactivation by UV-C light.

Abbreviations: CC, calcium carbonate; CFU, colony-forming units; D/A, data not available; MC, microcrystalline cellulose; NTU, nephelometric turbidity unit; PMMA, polymethyl methacrylate; RS, Ringer solution; SY, sunset yellow (dye); UV, ultraviolet; wA, with attenuator; woA, without attenuator; YPD, yeast-peptone-dextrose.

Practical Applications

UV-C treatment is a cold pasteurization process. It is a cost-effective alternative to the conventional heat treatment. The inactivation of organisms only occurs when they are directly exposed to the UV-C light. Liquid foods rather are suspensions than solutions. The presence of suspended particles can significantly reduce the efficacy of the treatment. It is imperative to understand the effect of suspended particles on process efficiency.

KEYWORDS

Mie scattering, Rayleigh scattering, *Saccharomyces cerevisiae*, turbid liquid food systems, turbulent flow, UV-C treatment

1 | INTRODUCTION

Liquid foods, such as juices, are commonly thermally processed to achieve microbial stabilization and extended shelf life. The pasteurization process is often accompanied by a change in color and a loss of nutritional value in the juices. Wines are stabilized by adding sulfur dioxide, but consumer acceptance of sulfites in wine is decreasing (Gama & Sylos, 2007; Pascal et al., 2020) Accordingly, the product should be minimally treated and without artificial additives, not least because of possible risks of food allergies. The inactivation of microorganisms with UV-C technology is an alternative or supplementary treatment method to conventional thermal processes or chemical additives.

Many liquid foods are rather turbid dispersions than clear solutions. The penetration and distribution of UV-C light in a liquid are affected differently by dissolved substances than by dispersed particles. The efficiency of a UV-C treatment is dependent on the uniformity of the dose distribution in the liquid. Besides the reactor design, the dose distribution depends on the penetration depth of the UV light into the liquid (Koutchma & Parisi, 2004). How far the light penetrates the liquid depends mainly on two effects: absorption and scattering. The gradual reduction of light in an absorbent medium can be described with the Lambert–Beer law:

$$I(d) = I_0 \times 10^{-\alpha l} \tag{1}$$

where I is the intensity of the light, α is the decadic attenuation coefficient, and l is the optical pathlength. The decadic absorption is defined as $A = \alpha l$. It is important to note that other publication also use the base e for the calculations of the absorbance coefficient. The Lambert–Beer law is only valid for solutions and not for dispersions (Swinehart, 1962).

In this study, the authors differentiate between the terms absorption and optical density in order to consider the effects of soluble and dispersed particles separately. The term absorbance A is only used for solutions. The term optical density OD is only used for the extinction of dispersions.

Mamane et al. (2006) showed that adding aluminum particles to a solution increases the extinction in a photometric measurement. In contrast, the absorbance remained the same when measured with an integrated sphere, where scattered light is captured. The scattering of light is usually an elastic process, in which the energy of the light is not substantially changed, only the direction of the light. How much of the light is scattered and in which direction depends on the ratio of particle size d_p to the wavelength λ of the incident radiation. Models of light scattering can be divided into different domains based on this ratio:

1. $d_p \gg \lambda$: geometrical optics
2. $d_p > \lambda$: geometrical scattering or Fraunhofer diffraction
3. $d_p \approx \lambda$: Mie scattering
4. $d_p \ll \lambda$: Rayleigh scattering

The scattering cross section C_{sca} of a particle determines how much radiation is scattered in all directions by the particle. When a particle with a geometric cross section of A is hit by a uniform light beam of Irradiance I_0, the particle scatters an amount of power W_{sca} into all directions (Platt & Collins, 2014). The scattering cross section is defined as:

$$C_{sca} = \frac{W_{sca}}{I_0} \tag{2}$$

The scattering efficiency is defined as the ratio of the scattering cross section to the geometric cross section:

$$Q_{sca} = \frac{C_{sca}}{A} = \frac{I_{sca}}{I_0} \tag{3}$$

Interferences dependent on the ratio of particle size and incident wavelength occur within the domain of Mie scattering interferences. The scattering efficiency can assume a value up to four times higher than the geometrical cross section.

The scatter efficiency also depends on the refractive index n' of the particle as well as the refractive index of the surrounding fluid.

$$n' = n - ik \tag{4}$$

The propagation speed and wavelength of incident light are influenced by the real part n of the refractive index. The Mie resonances

exhibit a strong dependence on the real part. The imaginary part characterize the attenuation of the wave. A particle with a high imaginary part is capable of absorbing a significant portion of incident light, as opposed to scattering it. Suspended particles have the potential to induce turbidity. Turbidity refers to the haziness in a fluid caused by dispersed particles, droplets, or bubbles. This phenomenon is rooted in the perception of the human eye. Turbidity is measured in Nephelometric Turbidity Units (NTUs).

Several studies have been conducted to investigating the UV-C inactivation in turbid food products, including fruit juices, wines, and cider. Table 1 presents a compilation of publications that have examined the inactivation of both clear or turbid liquid food products. Despite the fact that numerous studies have investigated inactivation in turbid media, there is a dearth of research on the same food matrix with and without turbidity agents. Kaya and Unluturk (2016) compared the inactivation of *Saccharomyces cerevisiae* among other organisms in clear and turbid grape juices using laminar tube flow. The study revealed that the inactivation of *S. cerevisiae* was more efficient in clear grape juice than in the turbid on. However, the authors compared two totally different juices, a commercial grape juice with an absorbance coefficient (254 nm) of 5.63 ± 0.01 cm^{-1} and a turbidity of 32.5 ± 0.14 NTU with a self-pressed grape juice with absorbance coefficient of 13.26 ± 0.02 cm^{-1} and a turbidity of 105.5 ± 2.12 NTU. Murakami et al. (2006) showed that the addition of 5 g/100 mL apple solids to a model solution containing a malate buffer altered the inactivation of *Escherichia coli K12*. A deviation in the slope of the inactivation rate was observed in the tailing of the curve. These experiments were conducted in a collimated beam system using petri dishes. It is important to note that the findings may not be directly applicable to flow-through reactor systems. Fenoglio et al. (2020) investigated the inactivation of *E. coli*, *Lactiplantibacillus plantarum*, and *S. cerevisiae* in clear pear juice, as well as in turbid orange-tangerine and orange-banana-mango-kiwi-strawberry juice blends. Here a annular thin film reactor with laminar flow conditions was used.

Cantwell et al. (2010) found no particle related shielding effect when disinfecting surface water in a pilot UV System with reduction equivalent dose of 90–100 mJ/cm^2. Although admittedly they only studied a turbidity up to 2 NTU. Loge et al. (1996) reported that suspended solids in waste water are the major cause for a tailing during UV-C treatment of *E. coli K12*. They investigated waste water with up to 18 NTU in a plug flow reactor. With the exception of Fenoglio et al. (2020) who have broadly specified a general particle size range of 0.1–1000 µm for all juices, none of the aforementioned studies have conducted a detailed characterization of the particles. To the best of the authors' knowledge, no studies have systematically investigated the influence of dispersed particles in food systems on the UV-C inactivation in flow-through reactors. The aim of this study was to investigate the impact of suspended particles on UV-C inactivation detached from the influence of absorption.

2 | MATERIALS AND METHODS

2.1 | Opacifiers

For the initial phase of this study five opacifiers were selected, namely microcrystalline cellulose (Merck AG, Germany), titanium dioxide (Carl Roth, Germany), silicon dioxide (S3 chemicals, Germany), polymethyl methacrylate (PMMA) spheres (Microbeads, Norway) and calcium carbonate (Carl Roth, Germany). In the second series of experiments, PMMA spheres of varying diameters were selected: 6 µm (Microbeads, Norway), 2.5 µm, 1.68 µm, 915 nm, 652 nm, 499 nm, 350 nm, 261 nm, 196 nm, and 104 nm (microParticles GmbH, Germany). Table 2 presents the refraction indices that are available for an incident radiation of 254 nm. There are only few sources providing information on refraction indices at a wavelength of 254 nm. The literature only provides information on the real part of silicon dioxide and calcium carbonate. The refractive index of cellulose at 254 nm was not found by the authors.

2.2 | Juices

Two commercially available juices were utilized in this study. Apple juice (naturtrüber Apfelsaft, REWE, Germany) and grape juice (naturtrüber Traubensaft, DM, Germany). The clarification process of the juices involved the addition of 1 mL of Ludox®PX30 (Deffner & Johann GmbH, Germany) per liter of juice. The juices were centrifuged at 10 G for 10 min and subsequently decanted. The clarification process resulted in a significant reduction in turbidity levels for both apple and grape juice samples. Specifically, the turbidity of the apple juice decreased from 2100 ± 124 NTU to 41.8 ± 12.8 NTU, while the grape juice turbidity decreased from 192 ± 19 NTU to 37 ± 10 NTU, as indicated in Table 3.

2.3 | UV-C technology

For this study, a reactor with turbulent flow conditions was selected. The UV-C treatment in turbulent flow has the highest efficiency (Hirt et al., 2022). The FDA approved the process specifically for turbulent flow, this is why most of the commercially used reactors such as the CiderSure® or SurePure® system use a turbulent flow regime. The reactor in this study was a modified UV-chamber model Opsytec BS04. The chamber was equipped with 20 dimmable (1%–100%) low pressure mercury lamps (Philips TUV F1T8, 16.7 W) with a power output of 4.5 W at 254 nm per lamps. A metal mesh can be placed beneath the lamps to function as an attenuator, thereby reducing the intensity of UV-C radiation. The reactor is equipped with 24 tubes made of fluorinated ethylene propylene, each measuring 62 cm in length, and installed beneath the UV-C lamps as illustrated in Figure 1. The tubes are interconnected using Tygon® tubes that are 14 cm in length and are not transparent to UVC radiation. This results

TABLE 1 Selection of studies investigating the UV-C inactivation of clear and/or turbid liquid foods.

Clear liquid food	Turbid liquid food	Reference
	Orange-tangerine blend	(Fenoglio et al., 2020)
	Orange-banana-mango-kiwi-Strawberry blend	(Ferrario et al., 2020)
Pear juice		(Fenoglio et al., 2020)
Grape juice	Grape juice	(Kaya & Unluturk, 2016)
Apple juice		(Ngadi et al., 2003)
		(Noci et al., 2008)
		(Gabriel & Nakano, 2009)
		(Koutchma et al., 2004)
		(Koutchma et al., 2004)
		(Murakami et al., 2006)
		(Keyser et al., 2008)
		(Guerrero-Beltrain & Barbosa-Canovas, 2005)
		(Char et al., 2010)
		(Ye et al., 2007)
		(Arroyo et al., 2012)
		(Tremarin et al., 2017)
		(Nicolau-Lapeña et al., 2022)
White grape juice		(Baysal et al., 2013)
		(Barut Gök, 2021)
	Orange juice	(Char et al., 2010)
		(Feliciano et al., 2019)
		(Gama & Sylos, 2007)
		(Oteiza et al., 2005)
		(Gayán et al., 2015)
		(Keyser et al., 2008)
		(Niu et al., 2021)
	Pineapple juice	(Mansor, 2014)
		(Rattanathanalerk et al., 2005)
	Watermelon juice	(Mansor, 2014)
Wine (white, rose, red)		(Junqua et al., 2020)
Grape must (different vines)		(Diesler et al., 2019; Fredericks et al., 2011)
Apple cider		(Basaran et al., 2004)
		(Geveke, 2005)
		(Duffy et al., 2000)
		(Quintero-Ramos et al., 2004)
		(Koutchma et al., 2004)
	Mango nectar	(Guerrero-Beltrán & Barbosa-Cánovas, 2006; Santhirasegaram et al., 2015)
	Carrot juice	(Jo & Lee, 2012)
	Almond milk	(Rathnayaka, 2012)
	Milk	(Barut Gök, 2021; Gök et al., 2021)
	Guava nectar	(Guevara et al., 2012)
	Passion fruit juice	
	Grapefruit	(Gabriel et al., 2017; Müller et al., 2011)

TABLE 2 Refraction indexes of the used opacifiers at 254 nm.

Material	Refraction index, *n*	Extinction coefficient, *k*	Source
Cellulose	N/D	N/D	
Titanium dioxide	2.5110	1.4992	(Siefke et al., 2016)
Silicon dioxide	1.5053	N/D	(Malitson, 1965; Tan, 1998)
PMMA	1.56[a]	0.001[a]	(Rashidian & Dorranian, 2014)
Calcium carbonate	1.8822	N/D	(Ghosh, 1999)
Water 20°C	1.3756	N/D	(Daimon & Masumura, 2007)

Note: N/D, no data available.
Abbreviation: PMMA, polymethyl methacrylate.
[a]Read from graphs.

TABLE 3 Properties of the turbid and clarified juices.

	OD, cm^{-1}	Turbidity NTU	Viscosity (20°C), mPa s	Density, $kg\,m^{-3}$
Apple juice + *Saccharomyces cerevisiae*	41.8 ± 12.8	2100 ± 124	1.61 ± 0.08	1045.34 ± 0.01
Clarified apple juice + *S. cerevisiae*	21.5 ± 4.7	53 ± 12	–	–
Grape juice + *S. cerevisiae*	18.8 ± 2.0	192 ± 19	2.84 ± 0.01	1068.86 ± 0.01
Clarified grape juice + *S. cerevisiae*	15.9 ± 0.3	37 ± 10	–	–

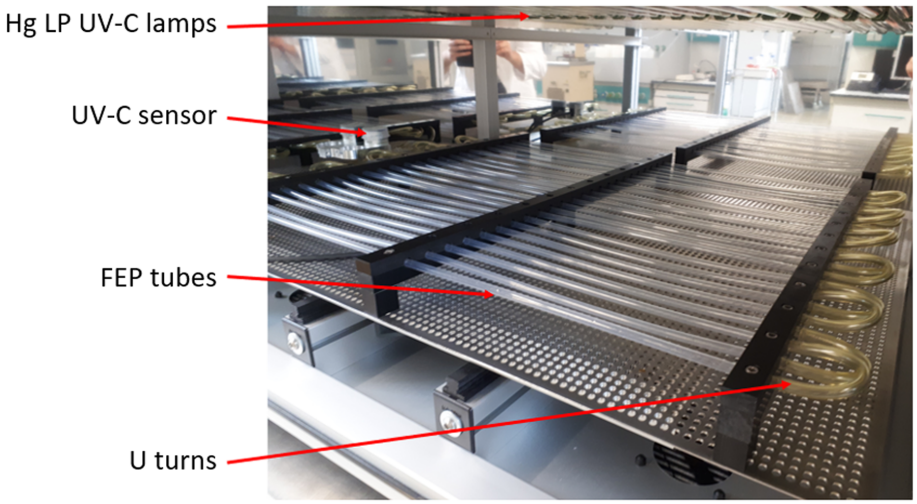

FIGURE 1 View into the modified BS04 UV chamber. The lamps are positioned 23 cm above the fluorinated ethylene propylene tube.

in a tube system that has a combined length of 18.10 m, with 14.88 m being capable of transmitting UV-C light. The distance between the lamps and the tubes is about 23 cm. The tube's inner diameter measures 6 mm, while its wall thickness is 0.3 mm. The flow regime within the tubes is characterized as turbulent, as evidenced by a Reynolds number of 5889, at a volumetric flow rate of 100 L/h. The chamber is outfitted with a sensor (Opsytech RM-12 sensor UVC) to quantify the intensity of UV-C radiation.

The treatment of the inoculated media and the actinometric solution was carried out as follows. Prior to treatment of the inoculated media and the actinometric solution, a warm-up phase of 45 min was implemented to establish stable conditions. During the warm-up phase, water tempered to 20°C was circulated through the reactor to mitigate any potential increase in reactor temperature. The ringer solution underwent sterilization, followed by the addition of opacifiers and/or color agent and yeast. The suspension was stirred. The resulting suspension was then tempered at a temperature of 20°C. Prior to pumping the solution through the reactor, the feeding peristaltic pump's tube (Heidolph Hei-FLOW Precision 06) underwent sterilization using Bacillol®. The suspension used for feeding was continuously agitated using a magnetic stirrer to avoid any sedimentation of particles. The first 200 mL of the effluent were discarded. At this point, a steady state of the UV-C process is reached and a 50 mL sample was extracted while the remaining suspension was collected in a fresh sterile bottle. This liquid was then used as the new feeding suspension and the process was repeated for each pass. The temperature was measured after each pass. Due to the distance between the lamps and the tubes and an airflow from bottom to top the temperature of the fluids did not raise more than 1.6 K after 6 passes.

In general, each inactivation was performed three times. The inactivation of *S. cerevisiae* in PMMA suspensions however was conducted only once, due to the high costs of the PMMA particles.

2.4 | UV-C dose measurement

To quantify the UV-C dosage absorbed by a liquid, a chemical iodide/iodate actinometer (Rahn, 1997) was used. A solution of 0.6 M potassium iodide and 0.1 M potassium iodate in 0.01 M borate buffer was subjected to irradiation. The progress of triiodide formation was monitored by spectrophotometry at 352 nm. The dose can be calculated using the following equation:

$$D_{act} = \frac{A_{352\,nm} \times P_{253.7\,nm}}{pl \times \phi \times \varepsilon_{352\,nm}} \quad (5)$$

where $A_{352\,nm}$ is the measured absorbance at 352 nm, $P_{253.7\,nm}$ is the number of joules per Einsteins of 253.7 nm photons (4.716×10^5 J einst^{-1}), pl is the path length of the cuvette (1 cm), ϕ is the quantum yield (effects per photon in mol einst^{-1}), and $\varepsilon_{352\,nm}$ is the molar absorption coefficient of triiodide at 352 nm (27,600 dm^3 mol^{-1} cm^{-1}). The temperature T_i dependent quantum yield was determined by the following equation:

$$\phi = 0.73 \times (1 + 0.23 \times [c_i - 0.577]) \times (1 + 0.02 \times [T_i - 20.7°C]) \quad (6)$$

where c_i is the concentration of triiodide. The UV-C dose per pass was determined through iodide-iodate actinometry at varying intensity levels of the UV-C lamps, while maintaining a constant volume flow of 100 L/h. The UV-C power was varied with (wA) and without (woA) the attenuator inserted into the UV chamber between 0.2 and 10.7 mW/cm^2. Figure 2 demonstrates a linear relationship between the actinometric dose per pass through the reactor and the UV-C irradiance measured by the UV-C sensor located inside the chamber. The UV-C dose per pass through the reactor D_{UV} can be adjusted within the range of $D_{UV}(P = 1\%, wA) = 5 \pm 1\,J/L$ and $D_{UV}(P = 100\%, woA) = 342 \pm 8\,J/L$ without impacting the flow conditions or the residence time (distribution).

2.5 | Microbial UV-C inactivation

Saccharomyces cerevisiae (EATON SIHA® Aktivhefe 7 (Rieslinghefe) *S. cerevisiae*, strain D 576) was cultured at 30°C in 100 mL YPD (10 g/L yeast extract, 20 g/L peptone, 20 g/L dextrose) nutrient broth on a shaking incubator (90 rpm) for 24 h. The nutrient broth containing *S. cerevisiae* was centrifuged, decanted and subsequently, the yeast was transferred into a Ringer's solution. The model medium or juice was inoculated with an approximate concentration of 10^6 colony-forming units per milliliter (CFU/mL). The media underwent treatment with UV-C light, following the procedure outlined previously.

To ascertain the microbial counts, the medium treated with UV-C underwent a tenfold dilution series in Ringer solution and was subsequently plated out. The culture medium employed was a YPD agar with antibiotics (25 µg/mL Kanamycin and 30 µg/mL Chloramphenicol). The inoculated plates were incubated at 30°C for a duration of 48 h, after which the colonies were counted. Microbial count determinations were performed in at least triplicates.

The inactivation curve of this *S. cerevisiae* strain can be effectively modeled using the Weibull Model (Hirt et al., 2022). The equation has been modified so that it is dependent on the UV-C dose, rather than the duration of exposure. The Weibull model is defined as

$$\log\left(\frac{N}{N_o}\right) = -\left(\frac{D_{UV}}{\delta}\right)^p \quad (7)$$

where δ is the UV-C dose acquired for the first log-level of inactivation, p is the shape parameter and describes downward concavity

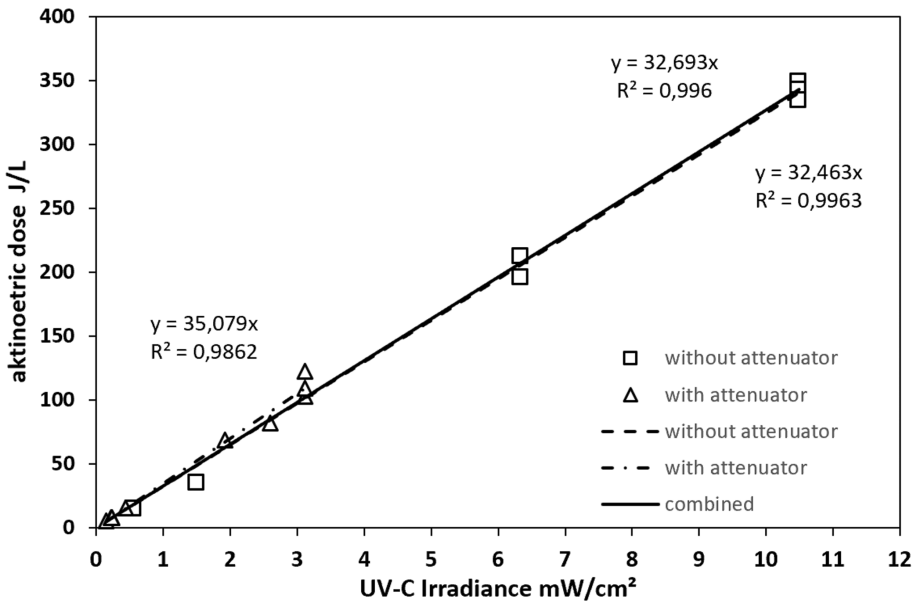

FIGURE 2 UV-C measurements per pass through the reactor with 100 L/h and different UV-C power levels.

($p > 1$) or upward concavity ($p < 1$) of the curve (if $p = 1$, curve is linear).

2.6 | Particle size distribution

The particle size distributions were determined with a Mastersizer 2000 (Malvern Panalytical) in Hydro 2000SM module (stirrer speed = 1500 rpm), software version 6.00 and the parameters indicated in Table 4. Mie theory was used for calculating the particle size distributions. Imaginary part of the refractive index was set to 0.01 according to Malvern Panalytical (Selecting an appropriate particle absorption for laser diffraction particle size calculations) for all samples except the PMMA particles. For PMMA imaginary parts of 26210E-07 (for 633 nm) and 20340E-07 (for 466 nm) were taken from (RefractiveIndex.Info, 2023a).

2.7 | Scanning electron microscopic images

For the scanning electron microscopy (SEM) images, the particles were dispersed in ultrapure water (Milli-Q IQ7000, Merck KGaA, Germany) before preparation. Since the different opacifier mixtures are not electrically conductive, the samples were sputtered with an approximately 5 nm thick platinum layer in a sputter coater (Q 150T ES, Quorum Technologies Ltd., UK). Powder and dispersion characterizations were performed in a field emission scanning electron microscope (FEI Quanta 250 Scanning Electron Microscope) with an Everhart–Thornley detector under high vacuum (pressure at about 0.0003 Pa) with an accelerating voltage between 5000 and 20,000 kV.

2.8 | Physical properties measurements

The optical density and absorbance were measured with a Unicam UV/VIS spectrometer in half micro UV-cuvettes with 1 cm pathlength (Brand GMBH + CO KG, Germany) with appropriate dilutions. The level of turbidity was quantified using a Turbiquant® 3000 IR. The pH value was measured using a WTW inoLab pH 720. The measurement of dynamic viscosity was conducted using a Thermo Scientific Haake MARS 60 rheometer. The density was determined using a flexural resonator (Heraeus/Paar DMA 60). All measurements were conducted in triplicates, and the means were calculated along with their corresponding deviations.

2.9 | Mie-calculations

For scattering calculation the Software MiePlot V4.6 by Philip Laven was used (Laven, 2021). The optical properties for the calculations are given in Table 2.

2.10 | Statistical analysis

Significance tests were conducted using the MS Excel ANOVA test with a confidence interval of $\alpha = 0.05$.

3 | RESULTS AND DISCUSSION

3.1 | Preliminary tests with different opacifiers

The initial set of experiments conducted aimed to investigate the influence of suspended particles on the UV-C inactivation of *S. cerevisiae*. Five insoluble substances were selected as opacifiers: micro crystalline cellulose, titanium dioxide, calcium carbonate, PMMA spheres ($d = 6$ µm) and silicon dioxide. The objective of the selection was to achieve a variety of physical properties, including variations in size, shape, and refractive index. Cellulose was selected as the material of choice due to its natural occurrence in the lees of juices and wines. Calcium carbonate and silicon dioxide are commonly used as adjuncts in the vinification process. The PMMA spheres were chosen, due to their spherical shape and the availability of different diameters. Titanium dioxide was used for it established function as a UV filter in sunscreen formulations. Figure 3 shows the SEM images of the opacifiers. It is evident that the sizes and shapes of the particles differ.

The particle size distribution is presented in Figure 4. PMMA, $CaCO_3$, and cellulose exhibit a monomodal distribution. The

TABLE 4 Parameters used for particle size analysis.

Material	Calculation model	Particle shape	RI at 633 nm	RI at 466 nm	Source for refractive index
PMMA	Single mode	Spherical	1.483	1.4929	(RefractiveIndex.Info, 2023a)
Titanium dioxide	General purpose–normal sensitivity	Irregular	2.68	2.88	(Malvernpanalytical, 2013)
Silicon dioxide			1.544	1.544	(Rawle, 2015)
Calcium carbonate			1.608	1.608	(Malvernpanalytical, 2021)
Microcrystalline cellulose			1.59	1.59	(Järvenpää, 2019)
Apple juice			1.4683	1.4780	Using refractive index for cellulose for the particles; refractive index for cellulose taken from (RefractiveIndex.Info, 2023b)
Grape juice			1.4683	1.4780	

Abbreviation: PMMA, polymethyl methacrylate.

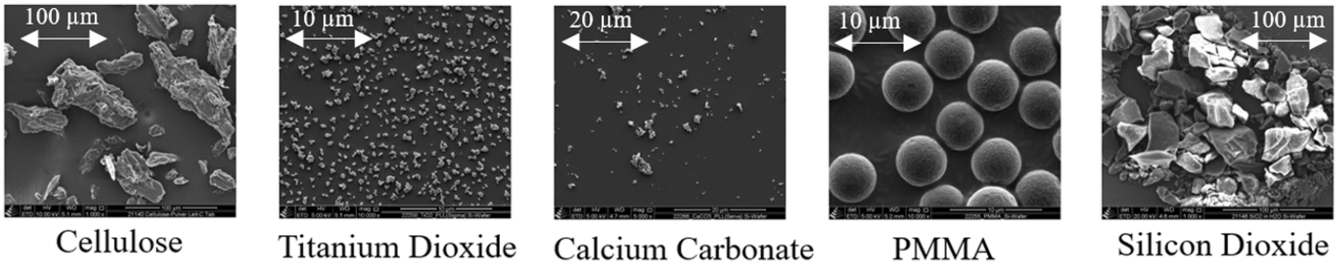

FIGURE 3 Scanning electron microscopic images of the opacifiers at the same magnification of 1:10,000. Scale is indicated with arrows.

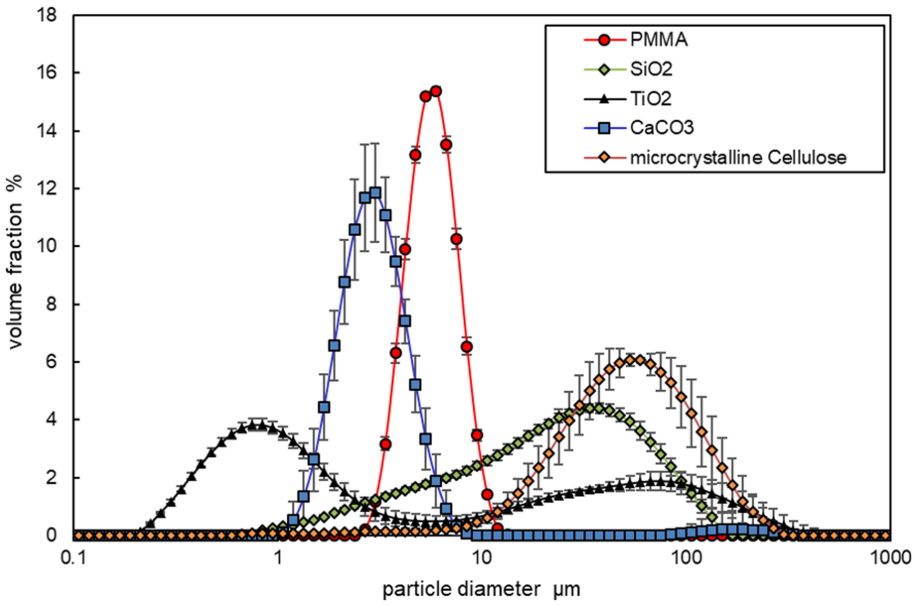

FIGURE 4 Particle size distribution of the five opacifiers measured using the Mastersizer 3000. Polymethyl methacrylate (PMMA), silicon dioxide (SiO_2), titanium dioxide (TiO_2), calcium carbonate ($CaCO_3$) and microcrystalline cellulose.

distribution of titanium dioxide exhibits two modes, with peak values observed at 850 nm and 75 µm Silicon dioxide shows a distinct peak at approximately 35 µm, accompanied by a secondary feature in the range of 1 to 10 µm. Titanium dioxide has the smallest particle size with a peak at approximately 850 nm, while cellulose displays the largest particle size with a peak at around 53 µm.

The model suspensions, comprising Ringer solution, sunset yellow and an opacifier, were adjusted to achieve an optical density of 10 for each suspension. Microcrystalline cellulose (MC) and calcium carbonate (CC) were used as opacifiers. Each experimental trial comprises of a control without the presence of an opacifier and a sample group containing varying concentrations of opacifier, specifically 100 NTU, 1000 NTU, and 4000 NTU. The weighing to achieve these turbidities are listed in Table 5. The absorption values presented in the table are attributed solely to the dye, without the presence of any particles. The turbidity is attributed to both the opacifiers and the yeast. The yeast population of 10^6 CFU/mL itself causes a turbidity of 18 ± 2 NTU, as observed in the control sample.

The initial experimental set demonstrates that the optical density of a suspension does not accurately indicate the potential efficacy of a UV-C treatment. Figure 5 shows the inactivation kinetics for the suspensions. The inactivation curves of each opacifier differ significantly $(\alpha = 0.05)$ from each other even so they have the same optical density.

The required dose δ for the first log level inactivation of *S. cerevisiae* determined from the Weibull fit correlates with the absorption of the liquid phase of the suspension as seen in Figure 6. The p parameter of the Weibull function showed no significant variation and was on average $p = 1.87 \pm 0.12$. The suspended particles used in this set of experiments seem to have little to no effect on the inactivation.

However, further investigation was required to explore a broader range of opacifiers. Consequently, model dispersions were formulated by incorporating all five opacifiers. Each dispersion consisted of Ringer's solution and a single opacifier without dye. The opacifiers were weighed in as listed in Table 6 to attain a turbidity level of approximately 1000 NTU.

The number of particles per liter ($N_{\text{particles}}$/L) was estimated with the density and the particle size distribution:

$$N_{\text{particles}} = \sum_{d_{\min}}^{d_{\max}} N_{d_i} = \sum_{d_{\min}}^{d_{\max}} \frac{V\%(d_i) \times m_p/\rho_p}{\frac{4}{3}\pi\left(\frac{d_i}{2}\right)^3} \quad (8)$$

The outcomes of the UV-C treatments are presented in Figure 7. As the experiments did not involve the addition of sunset yellow, the absorption of all model dispersions at 254 nm was zero. The

TABLE 5 Concentration of sunset yellow and the opacifiers microcrystalline cellulose (MC1–MC3) and calcium carbonate (CC1–CC3) to achieve a model suspension with an optical density at 254 nm of 10 cm^{-1}. The suspensions are number.

	Sunset yellow g/L	Absorption (254 nm)	OD	Microcrystalline cellulose g/L	Calcium carbonate g/L	Turbidity NTU
Control	0.173 ± 0.040	10.1 ± 1.0	10.1 ± 1.0	–	–	18 ± 2
MC1	0.164 ± 0.057	9.2 ± 0.7	9.9 ± 0.4	0.24 ± 0.09	–	107 ± 7
MC2	0.153 ± 0.053	8.6 ± 0.3	9.7 ± 0.5	1.64 ± 0.57	–	979 ± 30
MC3	0.094 ± 0.001	5.3 ± 0.4	10.0 ± 0.2	7.45 ± 0.1	–	4115 ± 44
CC1	0.166 ± 0.001	8.7 ± 0.6	10.2 ± 0.3	–	0.14 ± 0.01	92 ± 7
CC2	0.151 ± 0.031	7.4 ± 0.5	9.9 ± 0.8	–	0.62 ± 0.05	998 ± 24
CC3	0.072 ± 0.001	3.2 ± 0.6	9.9 ± 0.6	–	2.29 ± 0.06	4125 ± 198

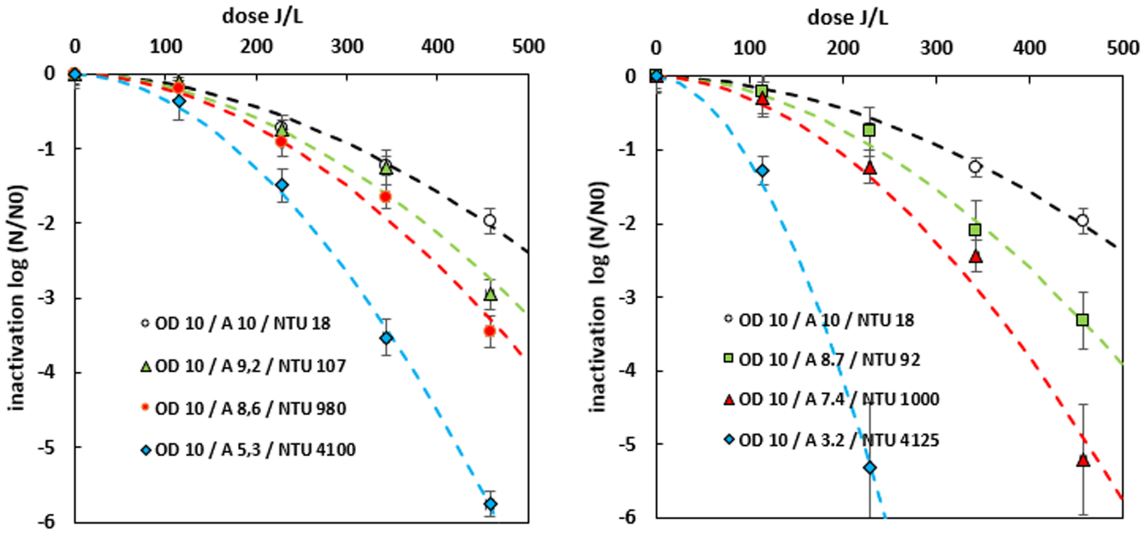

FIGURE 5 Inactivation of *Saccharomyces cerevisiae* in a model suspension consisting of Ringer solution (RS) with sunset yellow and the opacifiers microcrystalline cellulose (MC) (left) and calcium carbonate (CC) (right) in different compositions. All suspensions have an optical density of 10 at 254 nm. The dotted lines are the Weibull fits.

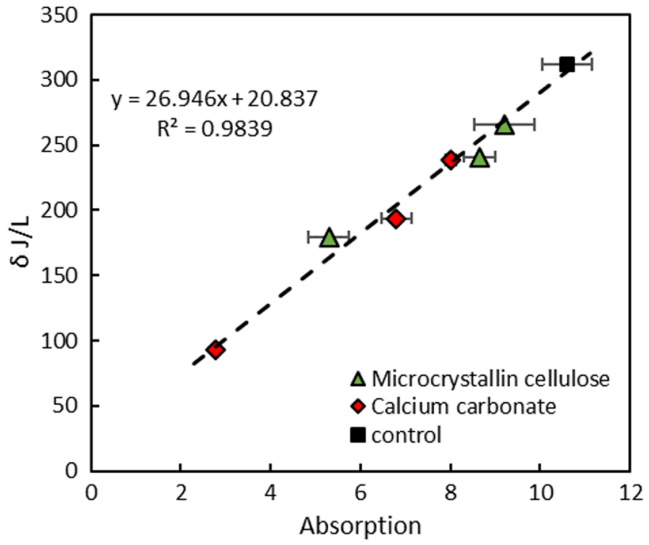

FIGURE 6 Required dose for the first log level reduction of *Saccharomyces cerevisiae* in the suspension of cellulose and calcium carbonate in different concentrations over the Absorption of the liquid phase of the suspensions (OD = 10 for all samples).

inactivation of *S. cerevisiae* in turbid media exhibits no significant variation from the control, except for the suspension containing titanium dioxide. Here the inactivation is far less effective compared to both the control sample and the other dispersions.

This outcome is not surprising, given that titanium dioxide is commonly employed as an UV-filter for example in sunscreen. Among the five opacifiers, titanium dioxide exhibits the smallest particle size but possess the highest extinction coefficient *k*. Therefor the particles absorb the UV-C light.

3.2 | Investigating the influence of the particle size of suspended particles on the inactivation of *S. cerevisiae*

The differences observed in the inactivation of *S. cerevisiae* in a TiO_2 suspension may be attributed to the size of the particles, the extinction coefficient, or a combination of both factors. The scattering rates and distribution of UV-C light are theoretically highly dependent on the size of the particles. To verify if this effect is noticeable in the

TABLE 6 Physical characterization of different suspensions consisting of Ringer solution, the opacifiers, and *Saccharomyces cerevisiae* 10^6 CFU/mL.

	SS g/L	OD, cm^{-1}	Turbidity NTU	Viscosity (20°C), mPa s	Density, $kg\,m^{-3}$	$N_{particles}$/L
RS + *S. cerevisiae*	0	0.17 ± 0.05	13.5 ± 4.1	1.00 ± 0.01	997.00 ± 0.01	0
RS + TiO_2 + *S. cerevisiae*	0.085 ± 0.018	0.27 ± 0.05	839 ± 20	1.07 ± 0.01	997.16 ± 0.01	1.31×10^{13}
RS + cellulose + *S. cerevisiae*	2.035 ± 0.001	0.93 ± 0.09	1226 ± 60	1.13 ± 0.04	997.40 ± 0.01	1.84×10^{11}
RS + SiO_2 + *S. cerevisiae*	4.824 ± 0.088	1.67 ± 0.39	1148 ± 12	1.13 ± 0.04	998.02 ± 0.01	2.05×10^{13}
RS + PMMA + *S. cerevisiae*	1.129 ± 0.088	1.20 ± 0.16	925 ± 84	1.11 ± 0.06	997.19 ± 0.01	1.4×10^{12}
RS + $CaCO_3$ + *S. cerevisiae*	0.607 ± 0.002	1.03 ± 0.57	1062 ± 61	1.31 ± 0.18	997.02 ± 0.01	2.25×10^{13}

Note: $N_{particles}$: Number of particles (estimated); Turbidity resulting in approximately 1000 NTU.
Abbreviations: PMMA, polymethyl methacrylate; RS, Ringer solution; SS, suspended solids.

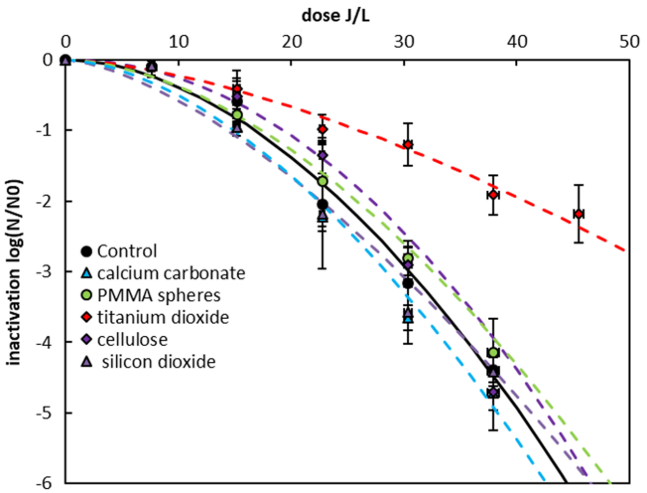

FIGURE 7 Comparison of inactivation curves of *Saccharomyces cerevisiae* in dispersions of ringer solution with different opacifiers with a turbidity of about 1000 NTU.

inactivation process, a series of experiments were executed with PMMA spheres ranging in diameter from 0.1 to 6 µm. The range of particle sizes encompasses both the Mie and Rayleigh scattering regimes. The diameters with their corresponding standard deviations are listed in Table 7. Figure 8 illustrates the computed scattering efficiency of PMMA in water at a temperature of 20°C as a function of particle size. The sizes of the PMMA particles have been indicated. The domains of Rayleigh and Mie scattering converge at a particle size of approximately 500 nm, assuming an incident light with a wavelength of 254 nm and a refractive index of 1.56–i0.001 (PMMA).

The amount of PMMA remains the same in all experimental runs: 0.265 g/L. Figure 9 the turbidity measurements obtained from the PMMA suspensions plotted against both the particle size and the scattering efficiency of 860 nm infrared light on PMMA in water. The suspensions containing PMMA particles with a diameter of 652 nm exhibit the highest level of turbidity, measuring at 940 ± 11 NTU. This finding implies that the turbidity measurements at a 90° angle are influenced by Rayleigh Scattering. This makes sense, because the Rayleigh scattering scatters light isotropically, whereas the Mie scattering scatters light in a forward direction. The phenomenon of Rayleigh scattering increases with the size of the scattering particle size until it reaches a point where it approaches Mie scattering. As a result, isotropic scattering is displaced by forward scattering.

The PMMA suspensions and the control were inoculated with a concentration of 10^6 CFU/mL *S. cerevisiae* and subsequently subjected to UV-C treatment. The figures depicting the inactivation curves of *S. cerevisiae* are presented Figure 10. The presented graph illustrates that the inactivation behaves differently depending on the size of particles in the suspensions. A particle size of 915 nm impedes UV-C inactivation the most. The Weibull model was applied to fit the inactivation curve for each inactivation curve. The parameters are presented in Table 7. The dose necessary to achieve a 5-log level reduction was calculated based on these parameters by rearranging Equation (7) to:

$$D_{UV} = \delta \times 5^{\frac{1}{p}} \tag{9}$$

Figure 11. displays the relationship between the scattering efficiency and the administered UV dose. There is no discernible variance in the inactivation process when particles are smaller than 500 nm and the scattering conforms to the Rayleigh domain. For particle sizes within the range of Mie scattering, there exists a correlation between the required dose and the scattering efficiency. The 915 nm PMMA particles in water have the highest scattering efficiency and the least efficient inactivation. The particles appear larger to the incident light than they physically are, so a greater proportion of the UV-C light is also scattered back. The penetration depth into the medium is smaller, and as a result, a smaller proportion is inactivated by the organism.

As there are next to no studies with a similar scope, it is not feasible to make a comparison with existing literature.

3.3 | UV-C inactivation in turbid and clear juices

UV-C inactivation in commercially available, turbid apple and grape juice was investigated in order to consider samples close to the application. The same juices were clarified to serve as control for a non-

TABLE 7 Physical properties of the PMMA suspension and the Weibull fit parameters for the UV-C inactivation of *Saccharomyces cerevisiae* in those suspension.

Particle size, µm	SS g/L	OD, cm^{-1}	Turbidity NTU	Weibull δ J/L	Weibull, p	R^2	Dose for 5 log-level inactivation J/L
0 (control)	0	0.1 ± 0.1	18 ± 2	16.8	1.84	0.994	44.3
0.105 ± 0.005	0.265	2.3 ± 0.2	187 ± 8	17.5	1.42	0.998	54.5
0.196 ± 0.004	0.265	4.0 ± 0.2	406 ± 12	12.0	1.15	0.990	48.5
0.261 ± 0.006	0.265	4.4 ± 0.2	681.5 ± 24	12.6	1.19	0.994	48.4
0.350 ± 0.008	0.265	5.5 ± 0.1	802 ± 9	13.2	1.22	0.992	49.4
0.499 ± 0.010	0.265	6.4 ± 0.4	921 ± 20	15.1	1.36	0.999	49.3
0.652 ± 0.018	0.265	6.8 ± 0.3	940 ± 15	15.5	1.15	0.999	62.4
0.915 ± 0.020	0.265	7.8 ± 0.5	831 ± 31	20.3	1.29	0.995	71.0
1.86 ± 0.04	0.265	1.7 ± 0.3	400 ± 7	17.9	1.45	0.997	54.1
2.5 ± 0.06	0.265	1.2 ± 0.3	332 ± 13	18.3	1.48	0.997	54.2
6.0 ± 1.2	0.265	0.2 ± 0.1	162 ± 3	17.4	1.76	0.999	43.5

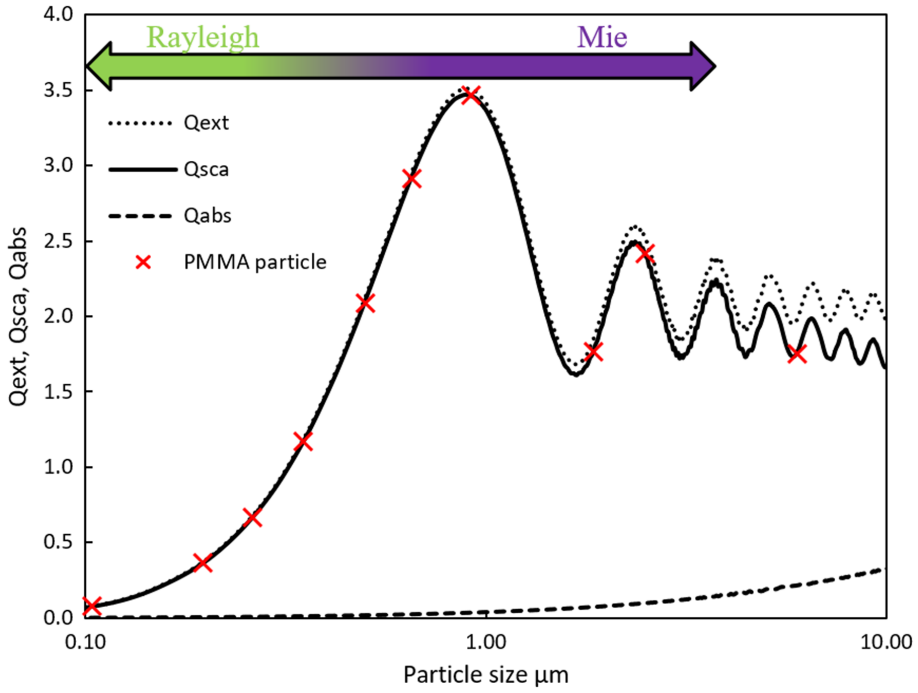

FIGURE 8 Scattering efficiency of polymethyl methacrylate (PMMA) in water at 20°C at 254 nm. Diameter of PMMA particles, used in this study, are marked.

turbid sample. The solids of the juices can be seen in SEM images in Figure 12. The size distribution of the juices is broad, as depicted in Figure 13, and exhibits multiple modes. The dominant peak of grape juice particles is observed at approximately 160 nm. The analysis of apple juice particles reveals the presence of two major peaks at 750 nm and 4.2 µm. Both juices contain particles larger than 100 µm.

The suspended solids in juices comprise a variety of substances, including proteins, (poly-)saccharides, pectin, and cellulose. The juice lees contain substances with varying refraction and extinction indices. In combination with the fact, that the particles are not spherical, it becomes nearly impossible to calculate the Mie Resonances. It is reasonable to anticipate that the maxima will occur within a comparable particle size range as that of the PMMA particles.

The turbid and clarified juices were inoculated with a concentration of 106 CFU/mL *S. cerevisiae* and subsequently subjected to UV-C

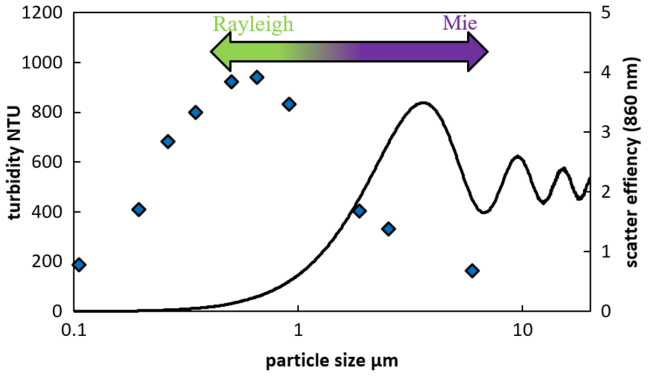

FIGURE 9 Turbidity of suspension consisting of polymethyl methacrylate (PMMA) spheres of different particle size in Ringer solution (all with the same concentration of 246 mg/L) and the scattering efficiency of PMMA spheres in water at 20°C at 860 nm.

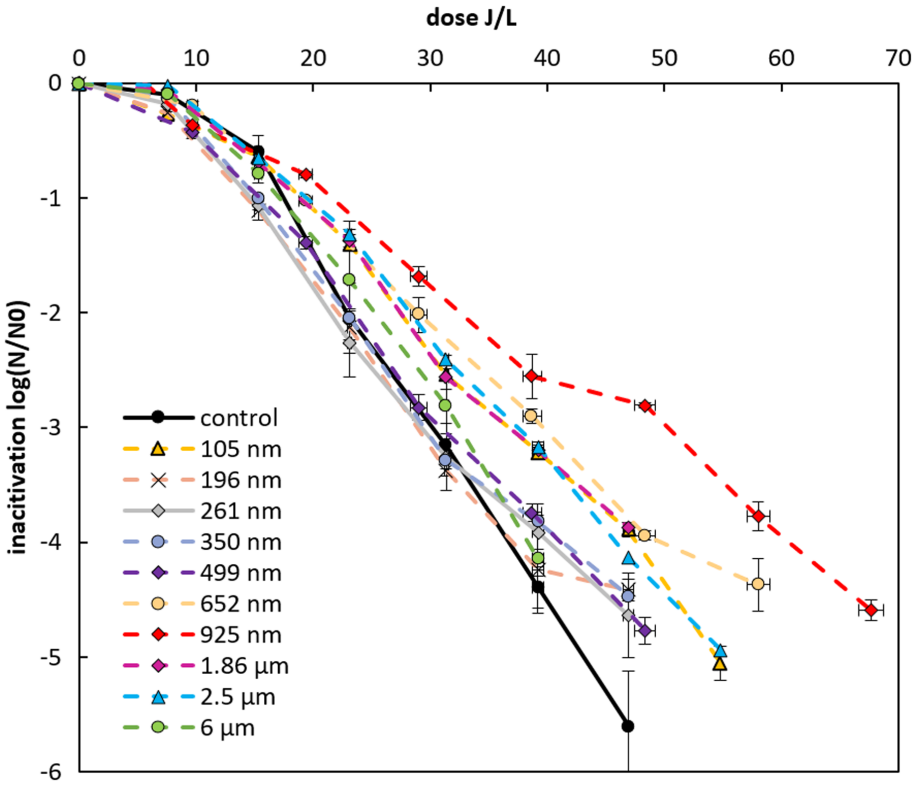

FIGURE 10 Inactivation curves of *Saccharomyces cerevisiae* in suspensions of Ringer solution and different sized polymethyl methacrylate (PMMA) (all in the same concentration of 0.264 g/L) particles in a turbulent flow.

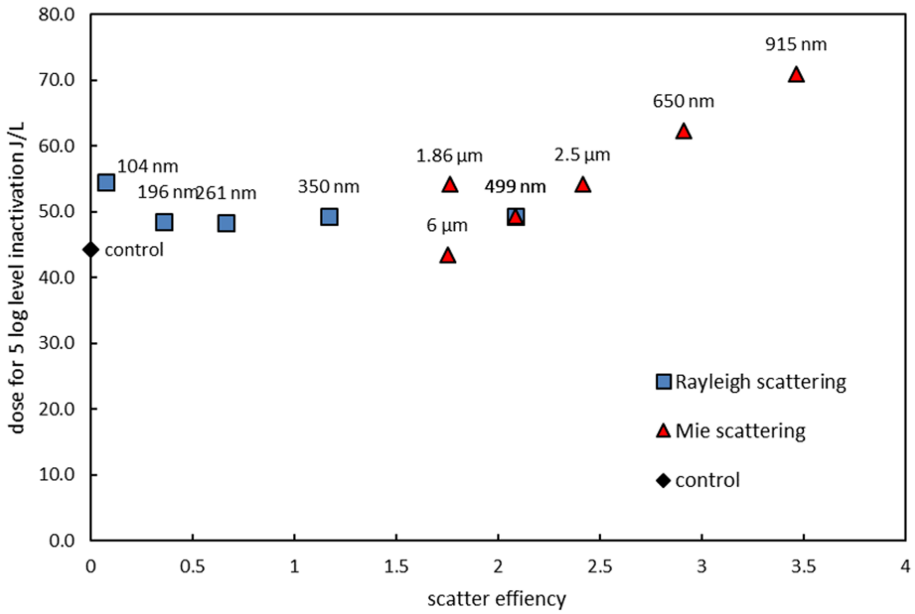

FIGURE 11 Dose required for a 5-log level inactivation of *Saccharomyces cerevisiae* in suspensions of Ringer solution and different sized polymethyl methacrylate (PMMA) spheres plotted over the calculated scatter efficiency of each particle. Mie and Rayleigh scattering are plotted separately.

treatment. The estimated doses for the first level of inactivation, as determined by the Weibull model, are $\delta_{\text{turbid apple juice}} = 1902$ J/L and $\delta_{\text{cleared apple juices}} = 1485$ J/L, respectively. The effect of UV-C treatment on turbid and clarified grape juices did not yield any statistically significant differences. The inactivation of *S. cerevisiae* in apple juice varies between turbid and clarified juices. This confirms the results presented in the model system studies. A significant proportion of particles found in apple juice fall within the size range of approximately 900 nm. The efficiency of inactivation is reduced as a result of a significant level of scattering. A greater dose is necessary to attain equivalent inactivation as that of the clarified counterpart, as illustrated in Figure 14.

This results coincide with the findings of Murakami et al. (2006), who added apple juice solids to a malate buffer. They found a deterioration in efficiency with a suspended solid content of 2.5 g/mL.

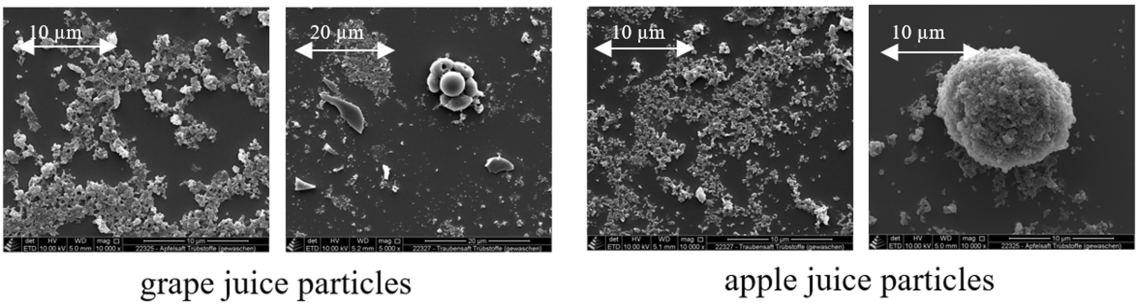

FIGURE 12 Scanning electron microscopic images of the juice particles (in the same 10,000× magnification).

FIGURE 13 Particle size distribution of suspended solids in turbid apple and grape juice measured using the Mastersizer 3000.

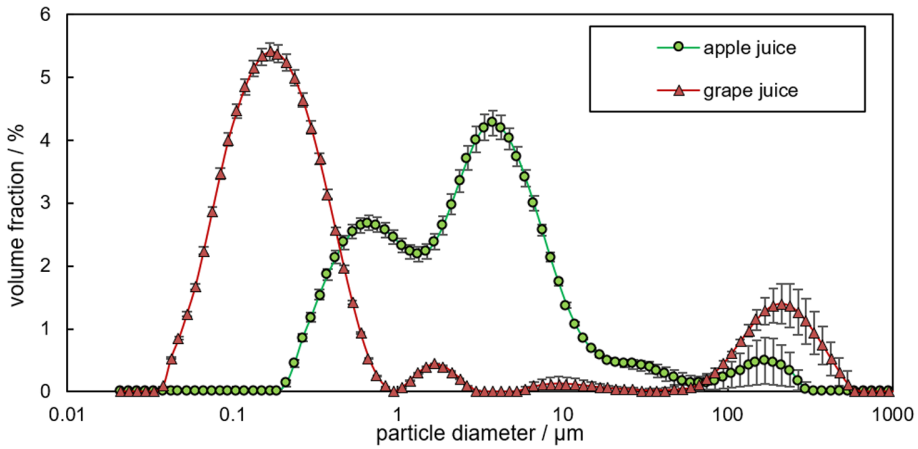

FIGURE 14 Comparison of the inactivation of *Saccharomyces cerevisiae* in turbid apple and grape juice to that of clarified ones in turbulent flow.

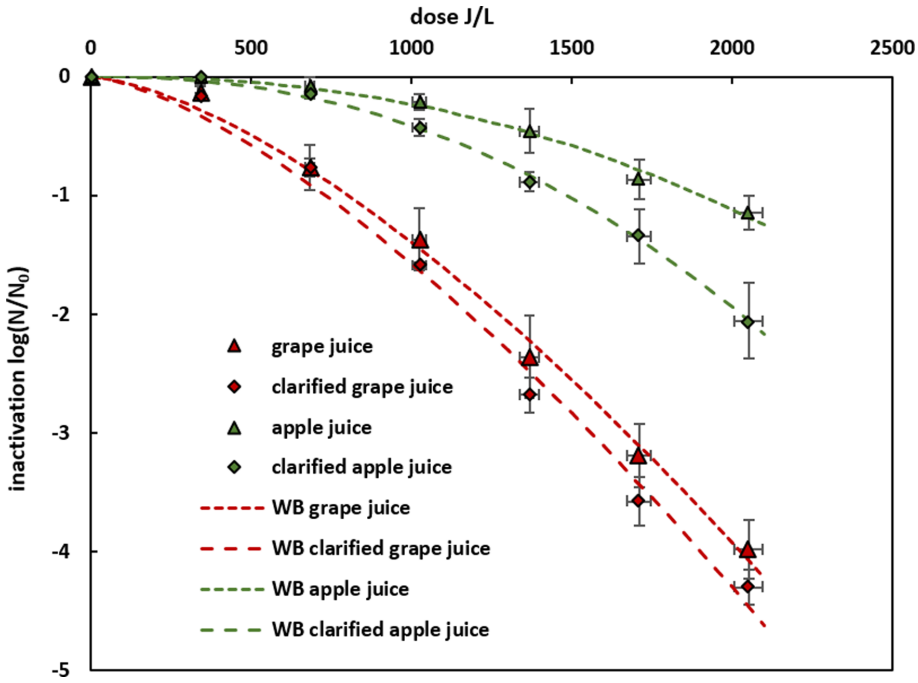

4 | CONCLUSIONS

This study shows that it is imperative to differentiate between a solution and a suspension to assess the effect on UV-C treatment. It is necessary to distinguish between the absorption of the liquid phase and the optical density of suspensions The measurement of suspended solids content or turbidity alone is inadequate for predicting the impact of suspended particles on UV-C inactivation. The turbidity

measurements are conducted using infrared light at 860 nm, thereby the respective scattering modes vary when compared to UV-C light at 254 nm.

Furthermore, it should be noted that the turbimeter solely detects and quantifies the intensity of light rays that have passed through the medium. UV-C light that exits the sample at a 90° angle would also have contributed to the inactivation of organisms.

The efficacy of UV-C inactivation of *S. cerevisiae* is significantly impacted by the particle size. When the size of particles is significant enough to cause Mie scattering and reach a resonance point, a higher dose of UV-C is required for inactivation. The impact of smaller particles, which induce Rayleigh scattering, on inactivation appears to be negligible. This is due to the fact that a greater amount of light is able to pass through the particles without any interaction, that is, less scattering of light. The second significant parameter to consider is the extinction coefficient of the particle. When a particle exhibits strong absorption, as in the case of titanium dioxide, the nature of scattering becomes less significant as absorption becomes the dominant factor in light extinction.

It is imperative to bear in mind that the interaction between UV light and particles occurs outside the realm of geometrical scattering. According to the principles of Mie and Rayleigh scattering, particles do not cast shadows behind themselves.

Further research is necessary to enhance comprehension of these effects. This study exclusively examined the species *S. cerevisiae*. Conducting a similar investigation on bacteria would be of significant interest. The modification of the liquid phase absorption in suspensions is necessary to investigate the correlation between these effects and the absorption liquid phase of the suspension. The Mie theory is exclusively applicable to spherical particles. Although the PMMA particles examined in this study exhibited a spherical shape, it should be noted that the majority of solid components present in liquid foods do not possess this morphology. This could result in a divergence between the actual scattering patterns and the theoretical counterparts.

AUTHOR CONTRIBUTIONS

Benedikt Woll: Writing–original draft, data curation, formal analysis, visualization, investigation, conceptualization, project administration. Volker Gräf: Writing–review & editing, conceptualization, funding acquisition. Svetlana Cvetkova: writing–review & editing. Maren Scharfenberger-Schmeer: Writing–review & editing, funding acquisition. Dominik Durner: Writing–review & editing, funding acquisition. Mario Stahl: Writing–review & editing, funding acquisition, supervision, conceptualization.

ACKNOWLEDGMENTS

We thank Veronika Larche, Claudia Csovcsics, Nele Weis, Luca Graf, and Christian Geuter for their excellent technical assistance. We thank Birgit Hetzer, Simone Brümmer. and Gunilla Breutmann for the SEM Image. We thank Jürgen Heinrich and Reiner Seitz for modifying the UV-C Chamber. Further we thank the FEI for their funding of this project. Open Access funding enabled and organized by Projekt DEAL.

CONFLICT OF INTEREST STATEMENT

The authors declare no conflicts of interest.

DATA AVAILABILITY STATEMENT

The data that support the findings of this study are available from the corresponding author upon reasonable request.

ORCID

Benedikt Woll https://orcid.org/0000-0002-0839-1945

REFERENCES

Arroyo, C., Gayán, E., Pagán, R., & Condón, S. (2012). Uv-C inactivation of *Cronobacter sakazakii*. *Foodborne Pathogens and Disease*, *9*(10), 907–914. https://doi.org/10.1089/fpd.2012.1178

Barut Gök, S. (2021). UV-C treatment of apple and grape juices by modified UV-C reactor based on dean vortex technology: Microbial, physicochemical and sensorial parameters evaluation. *Food and Bioprocess Technology*, *14*(6), 1055–1066. https://doi.org/10.1007/s11947-021-02624-z

Basaran, N., Quintero-Ramos, A., Moake, M. M., Churey, J. J., & Worobo, R. W. (2004). Influence of apple cultivars on inactivation of different strains of *Escherichia coli* O157:H7 in apple cider by UV irradiation. *Applied and Environmental Microbiology*, *70*(10), 6061–6065. https://doi.org/10.1128/aem.70.10.6061-6065.2004

Baysal, A. H., Molva, C., & Unluturk, S. (2013). UV-C light inactivation and modeling kinetics of *Alicyclobacillus acidoterrestris* spores in white grape and apple juices. *International Journal of Food Microbiology*, *166*(3), 494–498. https://doi.org/10.1016/j.ijfoodmicro.2013.08.015

Cantwell, R. E., Hofmann, R., Rand, J. L., Devine, P. M., & VanderMarck, M. (2010). Case study of particle-related UV shielding of microorganisms when disinfecting unfiltered surface water. *Water Quality Research Journal*, *45*(3), 343–351. https://doi.org/10.2166/wqrj.2010.030

Char, C. D., Mitilinaki, E., Guerrero, S. N., & Alzamora, S. M. (2010). Use of high-intensity ultrasound and UV-C light to inactivate some microorganisms in fruit juices. *Food and Bioprocess Technology*, *3*(6), 797–803. https://doi.org/10.1007/s11947-009-0307-7

Daimon, M., & Masumura, A. (2007). Measurement of the refractive index of distilled water from the near-infrared region to the ultraviolet region. *Applied Optics*, *46*(18), 3811–3820. https://doi.org/10.1364/AO.46.003811

Diesler, K., Golombek, P., Kromm, L., Scharfenberger-Schmeer, M., Durner, D., Schmarr, H.-G., & Fischer, U. (2019). UV-C treatment of grape must: Microbial inactivation, toxicological considerations and influence on chemical and sensory properties of white wine. *Innovative Food Science & Emerging Technologies*, *52*, 291–304. https://doi.org/10.1016/j.ifset.2019.01.005

Duffy, S., Churey, J., Worobo, R. W., & Schaffner, D. W. (2000). Analysis and modeling of the variability associated with UV inactivation of *Escherichia coli* in apple cider. *Journal of Food Protection*, *63*(11), 1587–1590. https://doi.org/10.4315/0362-028X-63.11.1587

Feliciano, R. J., Estilo, E. E. C., Nakano, H., & Gabriel, A. A. (2019). Ultraviolet-C resistance of selected spoilage yeasts in orange juice. *Food Microbiology*, *78*, 73–81. https://doi.org/10.1016/j.fm.2018.10.003

Fenoglio, D., Ferrario, M., Schenk, M., & Guerrero, S. (2020). Effect of pilot-scale UV-C light treatment assisted by mild heat on *E. coli*, *L. plantarum* and *S. cerevisiae* inactivation in clear and turbid fruit juices. Storage study of surviving populations. *International Journal of Food Microbiology*, *332*, 108767. https://doi.org/10.1016/j.ijfoodmicro.2020.108767

Ferrario, M., Fenoglio, D., Chantada, A., & Guerrero, S. (2020). Hurdle processing of turbid fruit juices involving encapsulated citral and vanillin addition and UV-C treatment. *International Journal of Food*

Microbiology, *332*, 108811. https://doi.org/10.1016/j.ijfoodmicro.2020.108811

Fredericks, I. N., Du Toit, M., & Krügel, M. (2011). Efficacy of ultraviolet radiation as an alternative technology to inactivate microorganisms in grape juices and wines. *Food Microbiology*, *28*(3), 510–517. https://doi.org/10.1016/j.fm.2010.10.018

Gabriel, A. A., Errol, J. O. A., & Tiangson-Bayag, C. L. P. (2017). Estimation of grapefruit juice color degradation from physicochemical properties and thermal inactivation parameters of *E. coli* O157: H7. *Philippine Journal of Science*, *146*(1), 65–79.

Gabriel, A. A., & Nakano, H. (2009). Inactivation of salmonella, *E. coli* and listeria monocytogenes in phosphate-buffered saline and apple juice by ultraviolet and heat treatments. *Food Control*, *20*(4), 443–446. https://doi.org/10.1016/j.foodcont.2008.08.008

Gama, J. J. T., & Sylos, C. M. d. (2007). Effect of thermal pasteurization and concentration on carotenoid composition of Brazilian Valencia orange juice. *Food Chemistry*, *100*(4), 1686–1690. https://doi.org/10.1016/j.foodchem.2005.01.062

Gayán, E., Serrano, M. J., Pagán, R., Álvarez, I., & Condón, S. (2015). Environmental and biological factors influencing the UV-C resistance of listeria monocytogenes. *Food Microbiology*, *46*, 246–253. https://doi.org/10.1016/j.fm.2014.08.011

Geveke, D. J. (2005). Uv inactivation of bacteria in apple cider. *Journal of Food Protection*, *68*(8), 1739–1742. https://doi.org/10.4315/0362-028x-68.8.1739

Ghosh, G. (1999). Dispersion-equation coefficients for the refractive index and birefringence of calcite and quartz crystals. *Optics Communications*, *163*(1), 95–102. https://doi.org/10.1016/S0030-4018(99)00091-7

Gök, S. B., Vetter, E., Kromm, L., Hansjosten, E., Hensel, A., Gräf, V., & Stahl, M. (2021). Inactivation of *E. coli* and *L. innocua* in milk by a thin film UV-C reactor modified with flow guiding elements (FGE). *International Journal of Food Microbiology*, *343*, 109105. https://doi.org/10.1016/j.ijfoodmicro.2021.109105

Guerrero-Beltrain, J. A., & Barbosa-Canovas, G. V. (2005). Reduction of Saccharomyces cerevisiae, *Escherichia coli* and listeria Innocua in apples juice by ultra violet light. *Journal of Food Process Engineering*, *28*(5), 437–452. https://doi.org/10.1111/j.1745-4530.2005.00040.x

Guerrero-Beltrán, J. A., & Barbosa-Cánovas, G. V. (2006). Inactivation of *Saccharomyces cerevisiae* and polyphenoloxidase in mango nectar treated with UV light. *Journal of Food Protection*, *69*(2), 362–368. https://doi.org/10.4315/0362-028X-69.2.362

Guevara, M., Tapia, M. S., & Gómez-López, V. M. (2012). Microbial inactivation and quality of guava and passion fruit nectars treated by UV-C light. *Food and Bioprocess Technology*, *5*(2), 803–807. https://doi.org/10.1007/s11947-011-0537-3

Hirt, B., Fiege, J., Cvetkova, S., Gräf, V., Scharfenberger-Schmeer, M., Durner, D., & Stahl, M. (2022). Comparison and prediction of UV-C inactivation kinetics of *S. cerevisiae* in model wine systems dependent on flow type and absorbance. *LWT*, *169*, 114062. https://doi.org/10.1016/j.lwt.2022.114062

Järvenpää, J. (2019). Suitability of microcrystalline cellulose as an ion exchanger: A radiochemical approach to the determination of ion exchange properties of AaltoCellTM materials. Helsingin Yliopisto; University of Helsinki; Helsingfors Universitet. https://helda.helsinki.fi/handle/10138/308240.

Jo, C., & Lee, K. H. (2012). Comparison of the efficacy of gamma and UV irradiation in sanitization of fresh carrot juice. *Radiation Physics and Chemistry*, *81*(8), 1079–1081. https://doi.org/10.1016/j.radphyschem.2011.11.070

Junqua, R., Vinsonneau, E., & Ghidossi, R. (2020). Microbial stabilization of grape musts and wines using coiled UV-C reactor. *OENO One*, *54*(1), 109–121. https://doi.org/10.20870/oeno-one.2020.54.1.2944

Kaya, Z., & Unluturk, S. (2016). Processing of clear and turbid grape juice by a continuous flow UV system. *Innovative Food Science & Emerging Technologies*, *33*, 282–288. https://doi.org/10.1016/j.ifset.2015.12.006

Keyser, M., Műller, I. A., Cilliers, F. P., Nel, W., & Gouws, P. A. (2008). Ultraviolet radiation as a non-thermal treatment for the inactivation of microorganisms in fruit juice. *Innovative Food Science & Emerging Technologies*, *9*(3), 348–354. https://doi.org/10.1016/j.ifset.2007.09.002

Koutchma, T., Keller, S., Chirtel, S., & Parisi, B. (2004). Ultraviolet disinfection of juice products in laminar and turbulent flow reactors. *Innovative Food Science & Emerging Technologies*, *5*(2), 179–189.

Koutchma, T., & Parisi, B. (2004). Biodosimetry of *Escherichia coli* UV inactivation in model juices with regard to dose distribution in annular UV reactors. *Journal of Food Science*, *69*(1), 14–22. https://doi.org/10.1111/j.1365-2621.2004.tb17862.x

Laven, P. (2021). MiePlot: A computer program for scattering of light from a sphere using Mie theory & the Debye series. http://www.philiplaven.com/mieplot.htm.

Loge, F., Emerick, R., Heath, M., Jacangelo, J., Tchobanoglous, G., & Darby, J. (1996). Ultraviolet disinfection of secondary wastewater effluents: Prediction of performance and design. *Water Environment Research*, *68*(5), 900–916.

Malitson, I. H. (1965). Interspecimen comparison of the refractive index of fused silica. *Journal of the Optical Society of America A*, *55*(10), 1205–1209. https://doi.org/10.1364/JOSA.55.001205

Malvernpanalytical. (2013). Particle size analysis of titanium dioxide using the Mastersizer 3000 laser diffraction particle size analyzer. https://www.malvernpanalytical.com/en/learn/knowledge-center/application-notes/an131216psatitaniumdioxideusingms3000.

Malvernpanalytical. (2021). Sample dispersion and refractive index guide (English). https://www.malvernpanalytical.com/en/learn/knowledge-center/user-manuals/man0396en.

Mamane, H., Ducoste, J. J., & Linden, K. G. (2006). Effect of particles on ultraviolet light penetration in natural and engineered systems. *Applied Optics*, *45*(8), 1844–1856. https://doi.org/10.1364/ao.45.001844

Mansor. (2014). Efficacy of ultraviolet radiation as a non-thermal treatment for the inactivation of salmonella typhimurium TISTR 292 in pineapple fruit juice. *Agriculture and Agricultural Science Procedia*, *2*, 173.

Müller, A., Stahl, M. R., Graef, V., Franz, C. M., & Huch, M. (2011). UV-C treatment of juices to inactivate microorganisms using dean vortex technology. *Journal of Food Engineering*, *107*(2), 268–275. https://doi.org/10.1016/j.jfoodeng.2011.05.026

Murakami, E. G., Jackson, L., Madsen, K., & Schickedanz, B. (2006). Factors affecting the ultraviolet inactivation of *Escherichia coli* K12 in apple juice and a model system. *Journal of Food Process Engineering*, *29*(1), 53–71. https://doi.org/10.1111/j.1745-4530.2006.00049.x

Ngadi, M., Smith, J. P., & Cayouette, B. (2003). Kinetics of ultraviolet light inactivation of *Escherichia coli* O157:H7 in liquid foods. *Journal of the Science of Food and Agriculture*, *83*(15), 1551–1555. https://doi.org/10.1002/jsfa.1577

Nicolau-Lapeña, I., Colás-Medà, P., Viñas, I., & Alegre, I. (2022). Inactivation of *Escherichia coli*, salmonella enterica and listeria monocytogenes on apple peel and apple juice by ultraviolet C light treatments with two irradiation devices. *International Journal of Food Microbiology*, *364*, 109535. https://doi.org/10.1016/j.ijfoodmicro.2022.109535

Niu, L., Wu, Z., Yang, L., Wang, Y., Xiang, Q., & Bai, Y. (2021). Antimicrobial effect of UVC light-emitting diodes against *Saccharomyces cerevisiae* and their application in Orange juice decontamination. *Journal of Food Protection*, *84*(1), 139–146. https://doi.org/10.4315/JFP-20-200

Noci, F., Riener, J., Walkling-Ribeiro, M., Cronin, D. A., Morgan, D. J., & Lyng, J. G. (2008). Ultraviolet irradiation and pulsed electric fields (PEF) in a hurdle strategy for the preservation of fresh apple juice. *Journal of Food Engineering*, *85*(1), 141–146. https://doi.org/10.1016/j.jfoodeng.2007.07.011

Oteiza, J. M., Peltzer, M., Gannuzzi, L., & Zaritzky, N. (2005). Antimicrobial efficacy of UV radiation on *Escherichia coli* O157:H7 (EDL 933) in fruit juices of different absorptivities. *Journal of Food Protection*, *68*(1), 49–58. https://doi.org/10.4315/0362-028X-68.1.49

Pascal, C., Dieval, J.-B., & Vidal, S. (2020). Predicting the post-bottling sulfite concentration evolution and wine shelf-life. *Internet Journal of Viticulture Ans Enology*.

Platt, C., & Collins, R. L. (2014). Lidar | Backscatter. In G. R. North, J. A. Pyle, & F. Zhang (Eds.), *Encyclopedia of atmospheric sciences: V1-6* (2nd ed., pp. 270–276). Elsevier Science. https://doi.org/10.1016/B978-0-12-382225-3.00205-X

Quintero-Ramos, A., Churey, J. J., Hartman, P., Barnard, J., & Worobo, R. W. (2004). Modeling of *Escherichia coli* inactivation by UV irradiation at different pH values in apple cider. *Journal of Food Protection*, *67*(6), 1153–1156. https://doi.org/10.4315/0362-028X-67.6.1153

Rahn, R. (1997). Potassium iodide as a chemical actinometer for 254 nm radiation: Use of Iodate as an electron scavenger. *Photochemistry and Photobiology*, *66*(4), 450–455. https://doi.org/10.1111/j.1751-1097.1997.tb03172.x

Rashidian, M., & Dorranian, D. (2014). Low-intensity UV effects on optical constants of PMMA film. *Journal of Theoretical and Applied Physics*, *8*(2). https://doi.org/10.1007/s40094-014-0121-0

Rathnayaka, R. (2012). The effect of ultraviolet and heat treatments on microbial stability, antioxidant activity and sensory properties of ready-to-serve tropical almond drink. *American Journal of Food Technology*, *7*(3), 133–141. https://doi.org/10.3923/ajft.2012.133.141

Rattanathanalerk, M., Chiewchan, N., & Srichumpoung, W. (2005). Effect of thermal processing on the quality loss of pineapple juice. *Journal of Food Engineering*, *66*(2), 259–265. https://doi.org/10.1016/j.jfoodeng.2004.03.016

Rawle, A. F. (2015). Best practice in laser diffraction – A robustness study of the optical properties of silica. *Procedia Engineering*, *102*, 182–189. https://doi.org/10.1016/j.proeng.2015.01.124

RefractiveIndex.Info. (2023a). Optical constants of (C5H8O2)n (Poly(methyl methacrylate), PMMA): Zhang et al. 2020: Tomson; n,k 0.4–20 µm.

RefractiveIndex.Info. (2023b). Optical constants of (C6H10O5)n (Cellulose): Sultanova et al. 2009: n 0.437–1.05 µm. https://refractiveindex.info/?shelf=organic&book=cellulose&page=Sultanova.

Santhirasegaram, V., Razali, Z., George, D. S., & Somasundram, C. (2015). Comparison of UV-C treatment and thermal pasteurization on quality of Chokanan mango (*Mangifera indica* L.) juice. *Food and Bioproducts Processing*, *94*, 313–321. https://doi.org/10.1016/j.fbp.2014.03.011

Siefke, T., Kroker, S., Pfeiffer, K., Puffky, O., Dietrich, K., Franta, D., & Tünnermann, A. (2016). Materials pushing the application limits of wire grid polarizers further into the deep ultraviolet spectral range. *Advanced Optical Materials*, *4*(11), 1780–1786. https://doi.org/10.1002/adom.201600250

Swinehart, D. F. (1962). The Beer-Lambert law. *Journal of Chemical Education*, *39*(7), 333. https://doi.org/10.1021/ed039p333

Tan, C. Z. (1998). Determination of refractive index of silica glass for infrared wavelengths by IR spectroscopy. *Journal of Non-Crystalline Solids*, *223*(1), 158–163. https://doi.org/10.1016/S0022-3093(97)00438-9

Tremarin, A., Brandão, T. R., & Silva, C. L. (2017). Inactivation kinetics of *Alicyclobacillus acidoterrestris* in apple juice submitted to ultraviolet radiation. *Food Control*, *73*, 18–23. https://doi.org/10.1016/j.foodcont.2016.07.008

Ye, Z., Koutchma, T., Parisi, B., Larkin, J., & Forney, L. J. (2007). Ultraviolet inactivation kinetics of *Escherichia coli* and *Yersinia pseudotuberculosis* in annular reactors. *Journal of Food Science*, *72*(5), E271–E278. https://doi.org/10.1111/j.1750-3841.2007.00397.x

How to cite this article: Woll, B., Cvetkova, S., Gräf, V., Scharfenberger-Schmeer, M., Durner, D., & Stahl, M. (2024). Systematic investigation of the influence of suspended particles on UV-C inactivation of *Saccharomyces cerevisiae* in liquid food systems. *Journal of Food Process Engineering*, *47*(1), e14520. https://doi.org/10.1111/jfpe.14520